On the design of test molds based on unidirectional saturated flows to measure transverse permeability in Liquid Composite Molding

Bin Yang[a,b], Wei Huang[c], Philippe Causse[d], Cédric Béguin[b], Jihui Wang[a], François Trochu[b,*]

[a] *School of Material Science and Engineering, Wuhan University of Technology, 122 Luoshi Road, Hongshan, 430070 Wuhan, PR China*

[b] *Department of Mechanical Engineering, Research Centre for High Performance Polymer and Composite Systems, Polytechnique Montréal, 2900 Boulevard Edouard Montpetit, Montréal, Québec H3T 1J4, Canada*

[c] *School of Civil Engineering, Wuhan University, 8 South Road of East Lake, Wuchang, 430072 Wuhan, PR China*

[d] *Department of Systems Engineering, École de Technologie Supérieure (ETS), 1100, rue Notre-Dame Ouest, Montréal, Québec H3C 1K3, Canada*

*Corresponding author

Abstract

Impregnating fibrous preforms through thickness has become a main feature of some *Liquid Composite Molding* process variants. Thus, the evaluation of transverse permeability is critical to optimize the fabrication and reduce manufacturing defects. Some problems connected with the design of testing devices need to be addressed to perform a reliable characterization. In this study, the efficiency of a typical one-dimensional testing device to measure transverse permeability is evaluated numerically and experimentally. The paper introduces a novel methodology to identify the optimal mold configuration and evaluate the flow pattern inside the mold cavity. A dimensionless number called the “fill coefficient” is also proposed to evaluate quantitatively the effect of the mold structure on the transverse flow pattern. The measured transverse permeability is shown to increase with lower fill coefficients for saturated and unsaturated flows. The intrinsic transverse permeability is obtained when the fill coefficient is equal to one. The proposed

methodology is verified by experiments performed in an existing tool. This confirms that the measured transverse permeability can be significantly affected by the above mentioned factors.

Keywords: Liquid Composite Molding, Mold deformation, Flow distribution, Preform, Transverse permeability

1. Introduction

Liquid Composite Molding (LCM) is a family of composite manufacturing processes, in which a liquid resin is injected into a mold cavity to impregnate a fibrous preform. Several new LCM process variants were developed over the years, such as vacuum-assisted *Liquid Resin Infusion* (LRI) with a distribution medium [1], *Compression Resin Transfer Molding* (C-RTM) [2] and *Flexible Injection* (FI) [3]. In these processes, an empty open space is filled by resin above the preform, followed by through-thickness impregnation. Therefore, knowledge of transverse permeability (K_z) is critical for process design and optimization, which characterizes the resistance of a fibrous preform to a transverse liquid flow through its thickness.

Thanks to its simplicity, the unidirectional test method is widely used to determine transverse permeability. In the latest international benchmark, twenty-eight experimental results were reported by 26 different participants, among which 22 were measured using this method [4]. This approach is carried out by establishing a unidirectional transverse flow through a stack of fibrous reinforcements (the “preform”) in the mold cavity. A typical example of a testing device is shown in FIGURE 1. The preform (white in the inset of FIGURE 1a) is laid out and compressed to the desired fiber volume fraction between two perforated plates (red). The test liquid or gas [5, 6] enters in the mold cavity from a bottom inlet gate, flows through the holes of the lower perforated

plate into the fibrous reinforcement, and then out of the sample through the upper perforated plate to leave finally the mold cavity from the outlet gate in the mold cover. The transverse permeability mold and data acquisition system provide experimental data (flow rate Q, pressure drop ΔP, etc.) to derive the K_z permeability from the one-dimensional Darcy's law [7]:

$$K_z = \frac{Q}{A} \cdot \frac{h_f}{\Delta P} \cdot \mu \quad (1)$$

where μ denotes the viscosity of the test fluid, A the flow area and h_f the thickness of the fibrous reinforcement (usually defined as the distance between the two perforated plates under and above the specimen).

Several unidirectional transverse permeability test molds have been described in the scientific literature to evaluate the transverse permeability of fibrous reinforcements [8-12]. However, the characterization of K_z remains a challenge. Differences of about two orders of magnitude were observed between experimental results with the same fibrous reinforcements and test liquid [4], although much lower variations (usually under 20%) are expected for measurements with the same measurement system. The observed discrepancy is due to several factors such as material variability, difference in test molds and measurement procedure. Another common source of error is the edge effect, namely the preferential boundary layer flow between the preform and the vertical cavity wall. This can be prevented by using specimens precisely cut with customized tools [13], adding seals on the sample perimeter [14-16] or considering separately the flow at the edge of the tested specimen [17].

Summing up the challenges reported in the scientific literature, the following issues appear:

1. Discrepancy in fiber volume fraction. Not much attention was paid in published articles to assess the possible deformations of the perforated plates due to pressure induced by sample clamping or liquid injection. This may change the thickness and fiber volume fraction of the specimen and hence alter its transverse permeability. Therefore, it is worth analyzing the deformation behavior to limit the fiber volume fraction discrepancy to an acceptable range when designing a new mold. Note that it can also be used to correct the cavity height of an existing mold.

2. Flow patterns in the cavity. In the one-dimensional method, calculating the transverse permeability by Darcy's law implies that the sample is considered homogeneous and crossed by a unidirectional transverse flow at the macroscopic level of Darcy's equation. Otherwise, as illustrated in FIGURE 2, an in-plane flow is involved, giving a flow rate generated by coupling the in-plane and transverse flows. The transverse permeability cannot be determined precisely in such a case. Fibrous reinforcements are usually not rigid enough to be self-supported. Therefore, support plates are introduced, which create a three-dimensional flow profile as shown in FIGURE 2. This affects the measured transverse permeability and might explain the poor reproducibility of test results for different testing devices. As a matter of fact, depending on the configuration of the test mold, the in-plane flow created varies from device to device. A parametric study is conducted in this article to connect partial unidirectional flows with K_z measurements. This leads to introduce a dimensionless number called the "fill coefficient" to evaluate the efficiency of test molds. A similar analysis is reported by Ferland et al. [18] for one-dimensional unsaturated in-plane permeability measurements, who showed that several

geometrical features in testing equipment might have a significant influence on the measured permeability.

3. Pressure drop of the test device. The pressure drop without specimen in an empty mold should always be negligible in front of the one created by the fibrous reinforcement. A similar verification was also carried out by Ferland et al. [18] for in-plane permeability measurements.

4. Material and/or specimen properties. The variability of measurements is usually attributed to discrepancies in textile architecture, nesting between plies and/or sample preparation. Up to now, not much attention was given to investigate the effect of other material properties such as that of the preform in-plane permeability on K_z measurements. However, the in-plane permeability of the fibrous reinforcement may play a role for anisotropic textile reinforcements because of the in-plane flow caused by perforated plates. Another concern is connected with the thickness of the specimen, which may affect the development of the flow pattern in the sample.

5. Effective flow area. Another difficulty is connected with the flow area A used in Eq. (1) to evaluate the transverse permeability since the flow is not perpendicular to the preform due to the presence of perforated plates. In the scientific literature, the flow area is usually referred to as the area of mold cavity cross-section [19], the actual open space [20], or a value between the two precedent ones [9, 21]. However, the methodology followed to determine the effective flow area was not fully investigated so far, although it can affect directly permeability. A similar investigation on effective flow area can be found in [22], which investigates the transverse gas permeability through prepregs.

6. Flow induced compaction. This issue studied by Klunker et al. [15] and Becker et al. [23] is based on Terzaghi's law [24], which states that the total stress applied to a porous material saturated with liquid is equal to the sum of pore pressure plus the load on its skeletal portion. Although a linear pore pressure profile is obtained according to Darcy's and Terzaghi's laws, nonlinear pressure distributions were observed by Klunker et al. [15] and Ouagne et al. [11]. Fluid induced compaction results in the highest fiber volume fraction at the outlet while the lowest appears at the inlet [15, 23].

This article focuses on the first four issues connected with the test mold (1, 2, 3) and with the dimension and anisotropy in permeability of the fibrous specimen (4). The investigation seeks to evaluate how the design of a unidirectional mold and material properties affect the accuracy of transverse permeability measurements. A new approach is proposed to assess the performance of unidirectional test devices while finding an optimal perforated plate design to minimize mold deformation. This could be possibly used to improve the reproducibility of tests performed with different molds. Since this work concentrates only on the impact of the test device on measurement accuracy, some causes of variability in measurements connected with the preform are neglected, such as nesting, local variability, edge effect and so forth. The analysis is performed at the macroscopic level of Darcy's equation. Namely, textile reinforcements are regarded as homogeneous porous media, and the microscopic uneven flow caused by their mesostructure is not considered. Besides, flow induced compaction is also neglected in experimental validations because the injection pressure used is much lower than the compaction pressure required to achieve the target fiber volume fraction.

In summary, the rest of this article is organized as follows. After a review of the scientific literature on transverse permeability in Section 2, investigation on mold deformation behavior is presented in Section 3. A relationship is proposed to connect the fiber volume fraction with preform compressibility and the open space ratio of the perforated plates to identify the optimal design configuration. In Section 4, parametric studies are conducted based on unsaturated and saturated flow simulations to evaluate a new dimensionless number, the "fill coefficient", devised to assess the performance of designed measurement tool. Section 5 presents an experimental verification on the accuracy of an existing K_z mold. The main results are summed up in Section 6 to provide guidelines to design more robust K_z test molds based on through-thickness flows.

2. Review of literature

Transverse permeability test devices based on one-dimensional Darcy's law are usually made out of transparent plastic [8], aluminum [8, 9] or stainless steel [13, 25, 26]. The shape of the mold cavity cross-section can be constantly square or circular. Its size ranges from 79 mm to 150 mm [8, 11, 15, 21, 27-30]. Among the difficulties encountered in the design of unidirectional test molds, the deformation behavior and the effect of non-unidirectional flow patterns represent two main issues. This is connected with the configuration of perforated plates, which turns out to be a critical feature in unidirectional test molds. Inappropriate evaluation of the role of perforated plates may prevent from accurately controlling the global fiber volume fraction and alters the streamlines inside the mold cavity.

Table 1 summarizes geometrical configurations of perforated plates reported in the scientific literature, including the material, shape, thickness, size and density of perforations. No specific

optimization or analysis were reported on these existing devices so far. The packing pattern and size of perforations differ from one another. In most published articles on K_z permeability, the mold is considered to be sufficiently stiff [31] to control the cavity height. Although this may be the case, this analysis provides a model to identify the optimal configuration of perforated plates.

Local fiber volume fraction can also be disturbed significantly (up to 26%) as noted by Graupner and Drechsler [32], because the outermost preform layers may bend in the open spaces of the perforated plates when a compaction force is applied. These authors added a sintered metal porous plate between the perforated plates and the preform to prevent fiber bending. Comparing K_z results with and without the sintered porous structure, they concluded that changes in local fiber volume content can be neglected [17]. Nevertheless, the transverse permeability of sintered porous plates and of the measured fabric were not reported in their investigation. For this approach to be valid, the porous plate should be at least two orders of magnitude more permeable than the measured preform. In fact, no study was yet conducted on the minimum permeability of flow distribution layers, nor on a way to evaluate quantitatively, as proposed in this article.

The presence of perforated plates or other similar flow distribution media creates a three-dimensional flow profile as discussed above, because of the limited flow exchange area between the free flow and the porous specimen. This is not consistent with the theoretical background, the one-dimensional Darcy's equation, which is used to derive the transverse permeability from experimental data. Scholz et al. [10] studied the non-unidirectional flow by numerical simulations with LIMS software [33]. As illustrated in FIGURE 2, the liquid flow in the cavity is divergent instead of along the thickness direction. In order to eliminate the unwanted in-plane flow and generate a more unidirectional flow, Wu et al. [20] placed an impermeable Mylar sheet with a 2.54

cm (1 inch) hole in the center between every two fabric layers, while Li et al. [19] machined two different sizes of perforations in the perforated plates to increase its open space.

Another approach was reported in the scientific literature with highly permeable flow distribution layers laid out above and below the preform. Note that a metallic mesh [10, 13] or a screen [20] have been used for that purpose. However, the permeability of the distribution layer and the size of the grid should be balanced, because too coarse a grid could lead to nesting between the preform and the distribution layers [34]. Another difficulty with this approach stems from its possible deformation if the distribution layers are not sufficiently stiff.

In summary, most researchers assumed that the perforated plates are highly permeable and have no influence on the pressure drop [15, 31]. For the required unidirectional flow, some of the measures mentioned above were taken only intuitively. No index can be used to evaluate the performance of test molds so far. The combination of these effects leads to poor test reproducibility of transverse permeability, as confirmed by the significant differences observed in the latest transverse permeability benchmark [4].

3. Cavity deformation for unidirectional mold with perforated plates

The deformation of the perforated plates resulting from specimen compaction pressure or injection pressure may vary the average thickness of the specimen, and hence affect transverse permeability characterization, which is a function of fiber volume fraction. The more open spaces exist in the two perforated plates, the easier it is to establish a transverse flow. However, this reduces the stiffness of perforated plates and may cause significant cavity deformation. Conversely, insufficient open spaces increase the resistance to the flow, and introduce another drift in K_z

measurements. To keep a balance between the open spaces and cavity deformation, mechanical analysis is carried out here followed by flow behavior analysis in next section to assess a proper range of geometric parameters for appropriate design of K_z molds.

Different configurations of circular perforated plates are analyzed based on two design parameters: the thickness of the plate and the packing pattern of perforations. Compressibility results carried out for the two benchmark fabrics [4] are used to determine the typical range of compaction pressure. The fluid injection pressure was not considered. The fluid pressure is equally applied on both sides of perforated plate since the pressure drop at perforated plate is negligible. Then the deformation behavior of the mold cavity is evaluated by finite element analysis. Finally, a two-dimensional model based on dual kriging interpolation [34, 35] is proposed to take into account the average deflection of perforated plates and correct, if needed, the thickness of test samples. In the end, a corrected value of K_z permeability is obtained as a function of actual cavity height.

3.1 Compressibility of engineering fabrics

The two typical fibrous reinforcements are a non-crimp glass multi-axial fabric produced by Saertex (NCF, 45°/90°/0°/45°, areal density of 444 g/m^2) and a twill glass woven fabric supplied by Hexcel (WF, areal density of 295 g/m^2) [4]. Square pieces of 100 mm × 100 mm are cut and stacked visually with the same orientation. Both dry and wetted compressibility is measured using a universal test machine (UTM, CRT-30kN, Shenzhen Riger Instrument Co., Ltd). The preform was fully saturated with PMX-200-100cs silicone oil for saturated tests. The stress evolution after compliance correction is plotted in FIGURE 3 against fiber volume fraction in dry and wet modes. Each test is repeated five times and averaged. The upper and lower bounds of the error bars represent the maximum and minimum values for each set of experiments. Higher stiffness and

similar compaction response between the dry and wet tests can be observed in the behavior of the NCF glass fabric. In contrast, the wet compaction pressure of the less rigid WF fabric is much lower than the dry one due to lubricating effects. FIGURE 3 shows that 270 kPa of compression pressure is required to reach a fiber volume fraction of 57%. In practice, the fiber volume fraction of composite parts rarely exceeds this value. Therefore, the maximum effective stress acting on perforated plates is taken as 600 kPa ($> 540\,kPa = 270\,kPa\,/\,50\%$) in this analysis because the open space ratio in perforated plates stands usually around 50%.

3.2 Simulation of perforated plate deformation

Hexagonal packing patterns are used for the arrangement of perforations, because it allows achieving a larger open space ratio compared to square packing. The geometrical model, the finite element mesh and boundary conditions are shown in FIGURE 4a. Thanks to symmetry, only a one-sixth circular sector model needs to be used in the calculations. The mesh is fine enough to obtain a detailed representation of the stress distribution for each kind of perforations. Fixed boundary conditions are imposed on the edge (support width, see FIGURE 4a) and a uniform pressure is applied on the bottom surface. The plate considered in our analysis has a radius of 57 mm to support a sample with an area of 100 cm^2 in addition to the area required to fix the perforated plate. Two materials are investigated numerically with standard mechanical properties: aluminum (Young's modulus: 70.0 GPa; Poisson's ratio: 0.33) and stainless steel (Young's modulus: 190.0 GPa; Poisson's ratio: 0.265). Different configurations of perforated plates are obtained by adjusting the perforation spacing and size.

To estimate the fiber volume fraction, the mean deflection is calculated from the node displacements in the thickness direction predicted by numerical simulation. The mean deflection

of the aluminum perforated plates under an even-distributed load is plotted in FIGURE 4b as a function of thickness t and open space ratio φ. As the open space ratio increases and thickness decreases, the deformation shows a significant increasing trend. Moreover, thickness plays a more significant role than the open space ratio. The deflection increases significantly for a thickness lower than 6 mm.

In Table 2, the maximum and mean deflections are compared for different perforation spacing and diameters while keeping nearly similar ratios of open space. The deflections remain similar and independent of the perforation spacing and diameter for the aluminum and stainless steel perforated plates. Therefore, a deflection model for different perforation patterns may consider only one independent variable, namely the open space ratio, instead of two (hole spacing and diameter). Moreover, the maximum and mean deflections are shown to be inversely proportional to the elastic modulus of the materials.

After having obtained the mean deflections for each configuration from the stiffness analysis illustrated in FIGURE 4b, all the data points are used to construct a parametric model of cavity deformation $D_f(t, \varphi)$ in Eq. (2) below based on dual kriging parametric surface interpolation [34, 35]. The line vectors $k_1(t)$ and $k_2(\varphi)$ are vector containing the drift and covariance functions of each kriging profile, and T and M are the dual kriging matrices along each interpolating direction (see Appendix A for more details on parametric surface kriging). Numerical calculations of the mean deflection at 100 kPa were carried out for n = 17 thickness values $t_i \in [2, 10]$, $1 \leq i \leq 17$ and m = 7 open space ratios $\varphi_j \in [45\%, 60\%]$, $1 \leq j \leq 7$. A total of $n \times m = 119$ mean deflection data points (t_i , φ_j) are obtained for $1 \leq i \leq 17$ and $1 \leq j \leq 7$, which are stored in a 17×7 matrix D_{base}. More details on parametric surface interpolation based on dual kriging are given in Appendix A.

The average deflection $D_f(t,\varphi)$ in millimeter of perforated plates as a function of D_{base} (mm) writes as follows:

$$D_f(t,\varphi) = k_1(t)^{\,T} \cdot T^{-1} \cdot D_{\text{base}} \cdot M_\varphi^{-1} \cdot k_2(\varphi) \tag{2}$$

where $k_1(t)$, T are matrices consisting of functions of perforated plate thickness t in millimeter, M_φ^{-1} and $k_2(\varphi)$ are matrices consisting of open area of perforated plate φ as shown in Appendix A. Note also that the elastic analysis carried out by finite element approximation is linear with respect to the external load, namely here the uniform compaction pressure P (kPa) applied on perforated plates. Hence, the mean deflection of perforated plates depends linearly on P. Therefore, the compaction pressure P may appear in the deflection model as a linear coefficient as follows:

$$D_f(t,\varphi,P) = P \cdot k_1(t)^{\,T} \cdot T^{-1} \cdot D_{\text{base}} \cdot M_\varphi^{-1} \cdot k_2(\varphi)/100 \tag{3}$$

Thus, after taking into account the mean deformations of the two perforated plates, the corrected average cavity height becomes:

$$H = h_f + 2 \cdot D_f(t,\varphi,P) \tag{4}$$

Finally, the mean deflection of perforated plates gives the mean fiber volume fraction and transverse permeability, respectively:

$$V_f = \frac{n \cdot \rho_A}{H \cdot \rho} \times 100\% \tag{5}$$

$$K_z = \frac{Q}{A} \cdot \frac{H\,\mu}{P_{in} - P_{out}} \tag{6}$$

where n is the number of fabric layers, ρ_A the areal density of the fibrous reinforcement (kg/m^2), H the cavity height after correction (m) and ρ the fiber density (kg/m^3). The proposed correction models for V_f and K_z allow characterizing more accurately the transverse permeability. Note that only the central matrix D_{base} in Eq. (3) must be recalculated when the material of perforated plates changes. This model is implemented in Section 5 to illustrate its application to an existing *Kz* mold.

4. Through-thickness flow pattern

In this section, the flow pattern inside the mold cavity is investigated by taking into account the configuration of perforated plates and dimensional issues connected with the specimen. The geometrical models of the mold cavity generated for the stiffness analysis are used to conduct flow analyses in both unsaturated and saturated modes. A way to ensure the generation of quasi one-dimensional flow in the test mold is proposed, together with a quantitative criterion to evaluate the performance of transverse permeability test molds.

4.1 Theory

The analytical solution giving the fill time t_{1D} at constant pressure for fully unidirectional porous unsaturated flows writes as follows [18]:

$$t_{1D} = \frac{\left(1 - V_f\right)\mu}{2\,K_z \cdot \Delta P} \cdot {h_f}^2 \tag{7}$$

where V_f denotes the fiber volume fraction and h_f the thickness of the specimen. The liquid is constrained to flow through the open spaces in the perforated plates and through the open spaces in the fibrous reinforcement. The solid part of the plates limits contacts between the specimen and the liquid. This changes the pressure distribution in the sample and modifies the flow paths of

liquid particles during the experiment. Therefore, FIGURE 2 shows a non-fully unidirectional flow in the specimen. This changes the actual fill time of the fibrous sample compared to the one-dimensional solution of Eq. (7). Hence a new dimensionless number called the “fill coefficient” was introduced as the ratio of the actual impregnation time of the cavity from the holes of the lower perforated plate over the fill time required in a unidirectional impregnation to evaluate quantitatively the effect of perforated plates on the flow pattern.

Since the perforated plates cover the bottom and top of the preform, to fill the specimen, only the open spaces in the lower perforated plate is considered as inlet gates on the bottom plane of the sample and the holes in the upper perforated plate model vents on the top plane of the specimen. Mold filling simulation carried out with PAM-RTM [36] gives the time t_{sim} needed to fill the preform. Hence the fill coefficient was defined as:

$$F = \frac{t_{sim}}{t_{1D}} \tag{8}$$

Ideally speaking, unidirectional filling should be the fastest way to fill a fibrous preform with a surface runner as injection port on the bottom side of the test sample. Thus, the fill coefficient measures the relative mold filling efficiency with respect to a full unidirectional through-thickness impregnation. A fill coefficient greater than 1 indicates a lower efficiency compared to a perfectly unidirectional filling. Note that the efficiency of a transverse permeability test mold can also be affected by the in-plane permeability when a three-dimensional flow front profile is created. For anisotropic fabrics, it is possible to achieve the same efficiency as in the unidirectional filling because the surface layer of the preform act as a flow distribution medium. Locally, there is a skin effect with significant in-plane velocity, then flow becomes unidirectional when the distance to the plate increases (in the core of the preform). Therefore fill coefficient could also be used to

measure the deviation of flow from quasi-unidirectional and as an index to measure the accuracy of transverse permeability tests. It facilitates the comparison of flow patterns for different geometrical configurations of perforated plates, and hence allows evaluating the efficiency of a transverse permeability test mold with respect to this issue.

Note that saturated flow simulations are also carried out in Section 4.6 to show that the fill coefficient is also suitable to evaluate saturated flow patterns. It is important because the most common methods to measure *Kz* are based on one-dimensional saturated flows [13], although unsaturated tests have also been conducted by several investigators [4, 37, 38].

4.2 Geometrical models

(a) Geometrical models for unsaturated filling analysis

As shown in FIGURE 5a, the unsaturated filling analysis can be simplified in PAM-RTM as follows: a pressure boundary condition is assigned to the area in contact with the holes of the perforated plates, namely the inlet pressure is set at 100 kPa relative pressure, and the outlet at 0 kPa. The model is discretized using tetrahedral elements, and the fiber volume fraction is set to 50%. The viscosity of the test liquid is considered constant at 0.1 Pa·s. Convergence analysis was conducted before the parametric investigation to ensure the independence of the numerical solutions from the mesh size for the filling and saturated flow simulations.

(b) Geometrical models for saturated flow analysis

The transverse permeability is usually measured in saturated flow experiments, because of the difficulty of tracking a transverse flow front through thin laminates [4, 37]. Therefore, it is critical

to ensure that the fill coefficient can also accurately assess saturated flow patterns in the K_z molds. To verify this, steady state laminar flow simulations were also performed with the software ANSYS Fluent [39]. FIGURE 5b shows the 3D geometrical domain for saturated flow simulation. The mesh was refined around the perforations to improve accuracy. It considered not only the specimen (porous domain) like in filling simulations, but also the Hagen Poiseuille flow through cylindrical holes of the perforated plates. The thickness of the preform remains 7 mm. The z = 0 mm plane corresponds to the base of the fibrous sample on the inlet side, and the z = 7 mm plane lies on the top of the preform on the outlet side. The same material properties and boundary conditions are specified as in the unsaturated filling simulations. Besides, a no-slip wall boundary condition is specified on the inner circumferential wall surface of the cavity.

4.3 Effect of perforations

As the most widely used flow distribution media, perforated plates can affect the fluid exchange between the flows in the preform and in the empty cavity through the hole diameter, the width between holes and the packing pattern. To evaluate the effect of perforations, the open space ratio remains at a similar level for different plate configurations. Unless otherwise specified, hexagonal packing patterns of perforations in the perforated plates were used to achieve a maximum open space for the transverse flow. The parametric investigation conducted is summarized in Table 3, in which only the hole spacing and diameter change. The first configuration in Table 3 is chosen as a reference case to investigate the effect of width between holes. Various widths are selected by adjusting the distance between neighboring perforations. The thickness of the preform is supposed here to be 7 mm, and the preform is assumed to be isotropic with a principal permeability of 3.0 x 10^{-12} m^2.

FIGURE 6a plots the fill coefficients obtained for the cases of Table 3 as a function of the number of holes. The fill coefficient decreases from 7 to 3 from 127 to 583 perforations. When the hole spacing and diameter decrease, the fill coefficient decreases even if the open space ratio does not change. However, when the number of holes increases nearly five times, the fill coefficient drops only by 55%, but still remains much greater than one. Hence the in-plane flow is not significantly reduced. Note that the fabrication of perforated plates becomes then more difficult and expensive because of the reduced hole size and larger number of holes. In contrast, FIGURE 6b shows that a significant improvement can be obtained by reducing the support width as defined in FIGURE 4a. This is especially true for support widths lower than 4 mm. In this analysis, it was achieved by increasing the inter-hole distance. Note also that the fill coefficient becomes even lower than in the configuration with 583 small holes (see FIGURE 6a).

Most of the perforations encountered in the scientific literature follow a hexagonal packing pattern. The holes adjacent to the edge of the plate are not evenly distributed due to the limited area and need to reserve a space to hold the fixture (referred to as “support width” hereinafter). This results in more in-plane flow near the edge than in the center, and affects the flow pattern in the cavity. A perforated plate model with evenly distributed perforations near the edge was created as reference in FIGURE 7b. The central hole is located in the center of the plate, and the second round of perforations follow a hexagonal pattern. Starting from the third round, the number of holes doubles for each new round.

FIGURE 7 shows results of filling simulations for a 20 mm thick preforms (instead of 7 mm like in FIGURE 6) and displays the transverse velocity field inside the test cavity. When the preform is filled, the velocity field in the thickness direction appears in FIGURE 7c and FIGURE 7d.

Although the structure is asymmetric in Case a, the velocity field only slightly changes. In Case b, the velocity field in all cross-sections is almost the same. In both cases, the sudden change in velocity leading to a non-unidirectional flow mainly occurs near the edge of the cavity, but the affected area is larger in Case a. This shows that perforated plates with uniformly distributed holes near the edge, even with a larger hole diameter, decrease the fill coefficient from 1.58 to 1.31, and hence create a more unidirectional flow through the preform.

4.4 Effect of sample and material properties

In one-dimensional transverse permeability measurements, the geometrical dimensions and the flow properties of fibrous samples, namely here their thickness and in-plane permeability, are rarely taken into account in the analysis of transverse flows. For instance, the difference in measured transverse permeability for samples of different thicknesses is often attributed to nesting [8], while the in-plane permeability is generally ignored [21]. However, in-plane flows may occur due to the presence of perforated plates as shown in FIGURE 7c. For that purpose, perforated plates with holes of diameter 7.5 mm and a hole spacing of 8.5 mm as in the existing *Kz* mold of Section 5 were chosen to carry out numerical simulations. The open space ratio is 52.4% in this analysis.

a) Preform thickness

FIGURE 8a shows a top view of the geometrical model and plots the fill coefficient as a function of sample thickness. The flow domain in the preform was discretized with tetrahedral elements, and the vent was set at a relative pressure of 0 kPa (with respect to the atmospheric pressure). The principal permeability of the preform is isotropic with $K_x = K_y = K_z = 3.0 \times 10^{-12}$ m^2. The baseline

indicates a fill coefficient $F = 1$. As shown in this figure, when the thickness is less than 15 mm, F decreases significantly when thickness grows. If thickness continues to increase, the decrease of F slows down, but does not stabilize until the preform thickness reaches 50 mm. With the same configuration of perforated plates and boundary conditions, the velocity field is displayed in FIGURE 8b at the specified cross-section for preform thicknesses of 4 mm, 20 mm, and 70 mm respectively. This shows that the velocity inside the preform becomes more uniform for a larger specimen thickness. Hence, increasing the preform thickness to improve the one-dimensionality of the flow decreases the fill coefficient.

Moreover, since composite parts are mostly thin shell structures, it is worth keeping test samples as close as possible to the thickness of parts fabricated by resin injection. Therefore, using thick preforms is not necessarily recommended and the effect of thickness itself on transverse permeability, neglecting nesting, is worth to be investigated.

b) Preform in-plane permeability

Fibrous reinforcements may possess an isotropic or anisotropic flow behavior. The in-plane flow may play a significant role when the actual flow deviates from a unidirectional Darcy flow pattern since in-plane permeability is usually one or two orders of magnitude higher than the transverse permeability. The principal permeability values of the preforms analyzed here are summarized in Table 4. The thickness of specimens always remains 7.0 mm.

Table 4 shows that the fill coefficient is greater or approximately equal to one, but never less than one, even if the in-plane permeability is three orders of magnitude larger than K_z. Therefore, for an anisotropic preform with a larger in-plane than transverse permeability, the in-plane flow can

compensate for delays in fill times due to longer flow paths. Hence, when the fill coefficient nearly equals one for anisotropic preforms with larger in-plane than transverse permeability, this does not necessarily mean that the transverse flow is unidirectional. It only means that the measured transverse permeability is close to the value that would be measured in a perfectly unidirectional injection.

4.5 Flow distribution layer

The solid part of perforated plates is the main cause of the deviation from a quasi-unidirectional flow on the Darcy scale because it blocks the liquid flow and creates more complex flow patterns. Nevertheless, a rigid perforated plate is essential to precisely control the fiber volume fraction of fibrous samples since it is not rigid enough to be free standing. It is possible to use a Flow Distribution Layer (FDL) between the preform and the perforated plates to facilitate the spread of the liquid flow on the preform surface [10, 13].

To verify this hypothesis, a geometrical model with FDLs was created as illustrated in FIGURE 9. In addition to the yellow part representing the preform, two layers of elements (in pink and blue) are added to model FDLs of thickness 0.5 mm. The same boundary conditions are applied as in the previous analysis. The principal permeability of the isotropic preform is assumed to be 3.0 x 10^{-12} m^2 with a thickness of 4 mm. FIGURE 9 shows that the fill coefficient decreases significantly when the FDL permeability increases. The flow pattern becomes very close to the ideal unidirectional case with a fill coefficient close to 1 when the FDL permeability is three orders of magnitude larger than that of the fabric.

Note that a new problem may be introduced by the FDL because of possible nesting between the fabric and the FDLs. Huang et al. [13] developed an iterative algorithm to estimate the nesting depth between FDLs and fabric, Δh, from 3D images sequence generated by micro-CT scans. This approach was adopted in the present study to account for the nesting depth between FDLs and fabric when calculating the height *H* of the specimen as below:

$$H = h_f + 2 * D_f(t, \varphi, P) + \Delta h \tag{9}$$

Using *H* in Eq. (5)) and Eq. (6)) allows correcting the fiber volume fraction and the corresponding transverse permeability.

4.6 Saturated flow analysis

The FDL layers are modeled separately as porous zones under and above the 7 mm thick specimen. The same perforated plate configuration is used as in Section 4.4. In the porous zones, namely the preform and the FDLs, a source term S_i for the *i*-th (*x*, *y*, or *z*) momentum equation is added to Navier-Stokes equation [39]:

$$S_i = -\left(\sum_{j=1}^{3} D_{ij}\mu v_j + \sum_{j=1}^{3} C_{ij}\frac{1}{2}\rho|v|v_j\right) \tag{10}$$

where $|v|$ denotes the magnitude of the liquid velocity, D_{ij} and C_{ij} are prescribed 3 x 3 matrices representing the viscous and inertial resistances, respectively. In the case of a homogeneous preform with FDLs, we get:

$$S_i = -\left(\frac{\mu}{K}v_i + C_2\frac{1}{2}\rho|v|v_j\right) \tag{11}$$

where K and C_2 are the permeability and inertial resistance coefficients, respectively. The inertial resistance coefficient C_2 may be calculated by the following formula [40]:

$$C_2 = 2\frac{C_f}{\sqrt{K}} \tag{12}$$

where the principal permeability K of the isotropic preform is 3.0×10^{-12} m^2 and the dimensionless drag constant C_f = 0.55 [40]. In our case, the liquid velocity not being high (Reynolds number less than 1), the inertial resistance - the second term on the right hand side of Eq. (11) can be neglected compared to the viscous resistance (the first term on the right hand side of Eq. (11)).

Two cases without and with FDLs were simulated in FIGURE 10 and give fill coefficients of 5.1 and 1.1, respectively. The lower fill coefficient is obtained by adding FDLs of permeability K_{FDL} = 3.0×10^{-8} m^2 above and below the preform. FIGURE 10 displays the transverse velocity component w in the thickness direction along the z-axis by varying the transparency and colour as a function of velocity in the entire domain. When $F = 5.1$, the velocity in FIGURE 10c exhibits periodic values reflecting the periodic hole distribution. The velocity decreases gradually from the middle of the cavity to the edge. In contrast, when $F = 1.1$ as shown in FIGURE 10b, the distribution of the transverse velocity component w between the perforated plates exhibits a good uniformity except in the FDL layer, where it has a larger magnitude, hence facilitating the liquid flow through the bottom and top surfaces of the specimen.

The velocity component w along the z axis is extracted at z = 0.5 mm, 3.5 mm and 6.5 mm in both cases and shown in FIGURE 10c and FIGURE 10d. In these figures, the abscissa denotes the radius of the concentric circle where the sampling point is located. When $F = 5.1$, a very small velocity develops near the wall because of the impermeable edge of the perforated plate. The flow in the cross-sections z = 0.5 mm and z = 6.5 mm gets its maximum velocity in alignment with the center of the perforations, which is approximately equal to two times the minimum axial velocity in the

same cross-section. Even in the mid-surface of the specimen (z = 3.5 mm), the velocity component still fluctuates with the position of perforations, but with much less intensity.

In the case of FDLs, the velocity fluctuations in the three cross-sections are significantly reduced, and the velocity on the wall is only slightly lower than in the middle of the specimen (see FIGURE 10d). The velocity remains constant in the mid-surface of the preform (z = 3.5 mm). The cross-section view of the flow pattern in the mold cavity in FIGURE 10d shows that the liquid passes through the perforated plate and then quickly spreads out on the surface of the preform, thus creating a quasi-unidirectional flow in the specimen.

It is also worth noting that the flow rate is lower in the case of a larger fill coefficient. At the cross-sections where z = 0.5 mm, 3.5 mm and 6.5 mm, the average axial Darcy velocity is 0.35 mm/s, 0.34 mm/s and 0.37 mm/s when $F = 5.1$ compared to 0.42 mm/s, 0.42 mm/s and 0.43 mm/s when $F = 1.1$, respectively. The latter shows a good agreement with the analytical solution at 0.428 mm/s, obtained by Darcy's law, while a decrease of approximately 20% is observed in the mass flow rate for the former. Therefore, the measured transverse permeability obtained in that case is underestimated by 20%. This confirms the validity of the fill coefficient for transverse saturated permeability tests. It also confirms that the factors affecting the fill coefficient influence the accuracy of transverse permeability measurements as well.

4.7 Pressure drop in empty mold

The pressure drop in the K_z mold caused by an empty mold cavity with perforated plates was investigated by carrying out saturated numerical simulations. The same mold geometry as the one in Section 4.6 was tested. As a function of flow rate, the pressure drop in the empty mold was 21.5

Pa, 43.1 Pa, 64.6 Pa and 86.1 Pa for fluid velocities of 2 mm/s, 4 mm/s, 6 mm/s and 8 mm/s. To achieve the same injection velocity, a pressure gradient in the order of $10^5 \sim 10^6$ Pa/mm should be established in a typical textile reinforcements. The ratio of the pressure drop in the empty mold to that in typical textile reinforcements converges to a constant and keeps lower than 0.05%. Therefore, the pressure drop in an empty mold can generally be neglected.

5. Experimental verification

As introduced in Section 4, both saturated and unsaturated simulations show that longer flow paths than the specimen thickness are created because of the perforated plates. Therefore, the measured transverse permeability is significantly underestimated and can be evaluated by the proposed dimensionless number. The greater is the fill coefficient compared to 1, the more is the measured transverse permeability underestimated. Two sets of experiments with and without FDLs are conducted to verify this result. Using the average displacement of the perforated plates, the correction model of fiber volume fraction proposed in Section 3 is also applied here to demonstrate its use in one practical case. Note that in this case the average deformation of the test device is expected to be less than 0.5% of the preform thickness, because the transverse mold considered here was designed with the geometric parameters detailed in Section 3.

A *S*-glass satin weave fabric (SF) of areal density 220 g/m^2 from Nanjing fiberglass research and design institute is tested with PMX-200-100cs silicone oil, a substitute fluid specified in Benchmark III [4]. The fabric contains 18 tows/cm in the warp direction and 14 tows/cm in the weft direction. Each circular specimen has a diameter 114 mm and consists of 17 layers of SF fabric. The sample area is used as effective flow area to calculate the transverse permeability in all

tests. Fiber volume fractions are adjusted by different combinations of calibrated shims. A rigid metal screen was used as FDL to facilitate the flow distribution and reduce the fill coefficient in one group of the test. It is woven with metal wires of diameter 0.25 mm and regarded as non-deformable. There are 40 meshes per inch, and the size of each mesh is 0.385×0.385 mm. In the experiments with FDLs, one layer of FDL is placed below and one above the fibrous sample. Since the FDL mesh is miniature, nesting between the FDL and the fabric can be neglected ($\Delta h = 0$ in Eq. (9)).

The experiments use an existing tool made of 304 stainless steel shown in FIGURE 1. The injection pressure of 0.1 MPa is provided by a pressure pot and stabilized by a regulator. Commercial pressure sensors MIK-P300 with a specified accuracy of +/-0.25% for a range of pressure values from 0 to 0.6 MPa (Hangzhou Meacon Automation Technology, China) are installed near the outlet and inlet to monitor the liquid pressure in the cavity. A digital balance measuring mass accurately ($\pm$0.01g) up to 3000 g (AH-A+r, Shenzhen Anheng Electronic Weighing Apparatus Co., Ltd, China) is placed under the outlet to record the mass flow rate. The perforated plate is also made of 304 stainless steel with holes of diameter 7.5 mm, hole spacing of 8.5 mm and 52.4% open space ratio. The plate thickness is 7 mm. The upper and lower perforated plates are identical. The geometrical model of perforated plates given in Sections 5.4, 5.5 and 5.6 was devised from the geometry of this existing tool to facilitate the comparison of simulations with experiments.

Each series of tests was repeated five times. The average values are plotted in FIGURE 11 with the upper and lower bounds of errors bar representing the maximum and minimum values the five replicates. The average fiber volume fractions are 48.3%, 50.0%, 52.0%, and 53.7%, which correspond to sample thicknesses of 3.05 mm, 2.93 mm, 2.82 mm, and 2.72 mm, respectively.

FIGURE 11 shows that the measured transverse permeability with FDLs is between 20% to 30% larger than that without FDLs. This is consistent with the information inferred from the saturated flow analysis of Section 4.6. It also confirms that it is possible to disperse the liquid on the sample surface with FDLs, thus creating a quasi-unidirectional Darcy flow.

According to the compressibility test for the *S*-glass satin weave fabric, achieving the above mentioned fiber volume fractions requires an effective stress acting on both perforated plates of 231 kPa, 315 kPa, 435 kPa, and 611 kPa. Therefore, the deflection of each perforated plate can be calculated by Eq. (3) with the known structural parameters for the different pressure values. The corrected fiber volume fractions given by Eq. (5) are 48.2%, 49.8%, 51.8%, and 53.4%, which becomes 0.1%, 0.2%, 0.2%, and 0.3% smaller, respectively, than the nominal values. As expected, the correction on the fiber volume fraction for the mold considered here is rather small, especially because it was designed following the approach detailed in Section 3. This is not necessarily the case for all transverse permeability test molds.

FIGURE 11 shows in dash line the relationship between the fiber volume fraction and transverse permeability after correcting for the cavity thickness by Eq. (6). The corrected transverse permeability increases slightly. For perforated plates made of honeycomb or aluminum, the corrections on fiber volume fraction and permeability would be more critical.

Although the correction for deformation could be neglected for this test mold, the difference in FIGURE 11 between the experimental transverse permeability measured with and without FDLs is significant. The transverse permeability with FDL is 16.9%, 25.8%, 38.3% and 35.7% higher than these without FDL for fiber volume fractions of 48.2%, 49.8%, 51.8% and 53.4%,

respectively. This experimental observation is consistent with the results of the saturated flow simulations carried out in Section 4.6.

6. Conclusion

By limiting the investigation to Darcy flows, creating a quasi-unidirectional through-thickness flow in a fibrous preform is required to perform accurate transverse permeability measurements. As investigated in this article, the measurement accuracy is closely connected with the geometric structure of the test device. A new approach is proposed to assess the performance of unidirectional test devices while optimizing the design of perforated plates to minimize mold deformation. By providing general guidelines, this work can improve the accuracy of transverse permeability measurements.

The optimal configuration of perforated plates takes into account the deformation of the cavity under the mold clamping pressure and/or the injection pressure. The average deformation of the specimen was modelled as a function of the perforated plate thickness, the open space ratio and the compaction pressure. As illustrated in the experimental validation section, it can also be used to correct the cavity height in existing molds.

A numerical parametric study was conducted to assess the performance of unidirectional test devices. Mold filling simulations were carried out with PAM-RTM, and saturated flow simulations with Fluent. This showed that significant in-plane flows occur in textile reinforcements. As verified experimentally, this can underestimate transverse permeability by up to 30 % in the cases analyzed. Thus, a new dimensionless number called the “fill coefficient” was proposed to measure the relative filling efficiency of the mold compared to a full unidirectional through-thickness

impregnation and the accuracy of transverse permeability. Applying this approach for different device configurations, a fill coefficient greater than 1 indicates a lower efficiency than the unidirectional case. Besides, saturated flow simulations show that the fill coefficient is also suited to evaluate saturated flow patterns. This is important since the most common unidirectional methods are based on saturated flows. The results show that reducing the hole diameter, increasing the open space ratio, using a more uniform hole packing in the perforated plates and secondary *Flow Distribution Layers* (FDL) are possible corrective actions to improve the performance of the test device to create quasi-unidirectional flows. Among them, as verified by experiments, FDLs turn out to be the simplest and most effective solution. However, this requires ensuring that the permeability of the FDL is at least three orders of magnitude higher than that of the specimen. In addition, because of the in-plane flow caused by perforated plates, note that the thickness of the specimen and the in-plane permeability of the fibrous reinforcement may also affect the transverse permeability measurement.

Although with FDLs, it is possible to remain consistent with Darcy's law and measure the transverse permeability in quasi-unidirectional flow conditions, the selection of an appropriate FDL could be an interesting topic in future investigations. It need not only be metallic. Rigid porous foams (ceramic or else) could provide interesting alternatives to prevent nesting between the FDLs and the textile specimens. However, Graupner and Drechsler [32] reported that the same nesting problem also exists when perforated plates are used, which still remains an open problem.

Acknowledgments

This research was partially funded by the *Department of Mechanical Engineering* of Polytechnique Montreal and by the *Natural Sciences & Engineering Research Council of Canada* (NSERC) (Discovery Grant). Authors also gratefully acknowledge the financial support of the composite laboratory by the *Research Center for High Performance Polymer and Composite Systems* (CREPEC), the "*Fonds de recherche du Québec - Nature et technologies*" (FRQNT) and the *Department of Mechanical Engineering* of Polytechnique Montreal. Authors would like to express their sincere thanks to Christian-Charles Martel, technical assistant at Polytechnique Montreal, for his high quality support in the laboratory. This research was also partially funded at Wuhan University of Technology by *the Fundamental Research Funds for Central Universities* (2019-JL-003). The help of Hao Zhang, a master degree student at Wuhan University of Technology, is highly appreciated for the experiments.

References

[1] Sirtautas J, Pickett AK, George A. *Applied Composite Materials.* 2015;22(3):323-341.

[2] Pham XT, Trochu F. *Polymer Composites.* 1999;20(3):436-459.

[3] Causse P, Ruiz E, Trochu F. *Polymer Composites.* 2011;32(6):882-895.

[4] Yong AXH, Aktas A, May D, et al. *Composites Part A: Applied Science and Manufacturing.* 2021;148:106480.

[5] Shadhin M, Jayaraman R, Rahman M. *Polymer Composites.* 2021;42(11):5743-5754.

[6] Fauster E, Vierkötter C, Appel L, et al. *Polymer Composites.* 2018;39(9):3247-3258.

[7] Darcy H. 1856:1-9.

[8] Fang L, Jiang J, Wang J, et al. *Applied Composite Materials.* 2015;22(3):231-249.

[9] Swery EE, Allen T, Comas-Cardona S, et al. *Journal of Composite Materials.* 2016;50(28):4023-4038.

[10] Scholz S, Gillespie JW, Heider D. *Composites Part A: Applied Science and Manufacturing.* 2007;38(9):2034-2040.

[11] Ouagne P, Breard J. *Composites Part A: Applied Science and Manufacturing.* 2010;41(1):22-28.

[12] Rimmel O, May D, Mitschang P. *Polymer Composites.* 2019;40(4):1631-1642.

[13] Huang W, Causse P, Hu H, et al. *Polymer Composites.* 2020;41(4):1341-1355.

[14] Visconti IC, Langella A, Durante M. *Applied Composite Materials.* 2003;10(2):119-127.

[15] Klunker F, Danzi M, Ermanni P. *Journal of Composite Materials.* 2015;49(9):1091-1105.

[16] Alhussein H, Umer R, Rao S, et al. *Journal of Materials Science.* 2016;51(6):3277-3288.

[17] Graupner R, Drechsler K. *Processdings of 14th FPCM.* 2018.

[18] Ferland P, Guittard D, Trochu F. *Polymer Composites.* 1996;17(1):149-158.

[19] Li M, Wang SK, Gu YZ, et al. *Composites Science and Technology.* 2012;72(8):873-878.

[20] Wu CH, Wang TJ, Lee LJ. *Polymer Composites.* 1994;15(4):289-298.

[21] Merhi D, Michaud V, Kampfer L, et al. *Composites Part A: Applied Science and Manufacturing.* 2007;38(3):739-746.

[22] Kratz J, Hubert P. *Composites Part A: Applied Science and Manufacturing.* 2013;49:179-191.

[23] Becker D, Broser J, Mitschang P. *Polymer Composites.* 2016;37(9):2820-2831.

[24] Schreyer L. *Computers and Geotechnics.* 1997;20(314).

[25] Li M, Gu YZ, Zhang ZG, et al. *Polymer Composites.* 2007;28(1):61-70.

[26] Trindade RS, Ribeiro AC, Souza JA, et al. *Polymer Composites.* 2019;40(10):3938-3946.

[27] Ouagne P, Ouahbi T, Park CH, et al. *Composites Part B: Engineering.* 2013;45(1):609-618.

[28] Aziz AR, Ali MA, Zeng X, et al. *Composites Science and Technology.* 2017;152:57-67.

[29] Liotier PJ, Govignon Q, Swery E, et al. *Journal of Composite Materials.* 2015;49(27):3415-3430.

[30] Studer J, Dransfeld C, Cano JJ, et al. *Composites Part A: Applied Science and Manufacturing.* 2019;122:45-53.

[31] Becker D, Mitschang P. *Advanced Composites Letters.* 2014;23(2):32-36.

[32] Graupner R, Drechsler K. 17th European Conference on Composite Materials: ECCM17-17th2016; Munich, Germany.

[33] Šimáček P, Advani SG. *Polymer Composites.* 2004;25(4):355-367.

[34] Huang W, Causse P, Brailovski V, et al. *Composites Part A: Applied Science and Manufacturing.* 2019;124(June).

[35] Trochu F. *Engineering with Computers.* 1993;9(3):160-177.

[36] Oliveira IRd, Amico SC, Souza JA, et al. Defect and Diffusion Forum2015.

[37] Konstantopoulos S, Grössing H, Hergan P, et al. *Polymer Composites.* 2018;39(2):360-367.

[38] Wu XQ, Li JL, Shenoi RA. *Journal of Composite Materials.* 2007;41(6):747-756.

[39] Fluent A. *Ansys Inc.* 2009;15317:1-2498.

[40] Ward J. *Journal of the hydraulics division.* 1964;90(5):1-12.

Appendix A – Model of plate deformation interpolated by parametric surface kriging

The deflection data obtained from the stiffness analysis at 100 kPa shown in FIGURE 4b are used to build a parametric surface interpolation model of the cavity deformation by parametric surface kriging [34, 35]. Deflection calculations were carried out for $n = 17$ thickness values $t_i \in [2, 10]$, $1 \leq i \leq 17$ and $m = 7$ open space ratios $\varphi_j \in [45\%, 60\%]$, $1 \leq j \leq 7$. A total of $n \times m = 119$ data points (t_i, φ_j) are obtained for $1 \leq i \leq 17$ and $1 \leq j \leq 7$. In kriging, a general correlation model between data points is constructed by assuming that the statistical correlation between observations (here the three parametric coordinates of surface points) depends only on their Euclidean distance h in the subspace of parameters $(t, \varphi) \in [2, 10] \times [45\%, 60\%]$, which is called the *intrinsic hypothesis* in kriging.

As illustrated in FIGURE 12, the thickness t of the perforated plate and the open space ratio φ are used as parameters along each interpolation profile so that the kriging interpolation can be directly expressed as a function of these two parameters. Two different correlation functions (also called

"generalized covariances" in kriging) $K_1(h)$ and $K_2(h)$ are used here for each variable t and φ respectively:

$$\begin{cases} K_1(h) = |h|^3 & : cubic\ covariance \\ K_2(h) = |h| & : linear\ covariance \end{cases}$$

The kriged interpolation proposed as deflection model of the perforated plates depends on the plate thickness and open space ratio φ as follows:

$$D_f(t,\varphi) = k_1(t)^{\,T} \cdot T^{-1} \cdot D_{\text{base}} \cdot M^{-1} \cdot k_2(\varphi) \tag{13}$$

where T and M are the dual kriging matrices along profiles 1 and 2, respectively:

$$T = \begin{bmatrix} & & & 1 & t_1 & t_1^2 \\ & |t_i - t_j|^3 & & \vdots & \vdots & \vdots \\ & & & 1 & t_n & t_n^2 \\ 1 & \cdots & 1 & 0 & 0 & 0 \\ t_1 & \cdots & t_n & 0 & 0 & 0 \\ t_1^2 & \cdots & t_n^2 & 0 & 0 & 0 \end{bmatrix} \quad M = \begin{bmatrix} & & & 1 & \varphi_1 \\ & |\varphi_i - \varphi_j| & & \vdots & \vdots \\ & & & 1 & \varphi_m \\ 1 & \cdots & 1 & 0 & 0 \\ \varphi_1 & \cdots & \varphi_m & 0 & 0 \end{bmatrix}$$

and the vectors of drift and covariance $k_1(t)$ and $k_2(\varphi)$ are defined as follows along each kriging profile:

$$k_1(t) = [|t - t_1|^3 \quad \cdots \quad |t - t_n|^3 \quad 1 \quad t \quad t^2]^T \tag{14}$$

$$k_2(\varphi) = [|\varphi - \varphi_1| \quad \cdots \quad |\varphi - \varphi_m| \quad 1 \quad \varphi]^T \tag{15}$$

The matrix D_{base} contains the deflection values at the positions (t_i, φ_j) for the 119 simulations performed at a given uniform compaction pressure of 100 kPa. The matrices T and M do not depend on the unknown deflection, but only on the finite number of parameter values selected as thickness and open space ratio to conduct the numerical simulations.

Figure list

FIGURE 6 Effect of two geometrical parameters on flow patterns for a 7 mm thick preform: (a) Number of perforations for nearly the same open space ratio and reduced hole diameters. (b) Support width (for simulations based on the configuration of Table 1). The decrease in support width is achieved by increasing the inter-hole distance).

FIGURE 7 Influence of hole packing calculated for a 20 mm thick preform: (a) Non-uniform distribution of perforations near the edge of the mold cavity. (b) Uniformly distributed perforations. (c) Vertical transverse velocity fields in the XZ and YZ planes in Case a. (d) Vertical transverse velocity fields in the XZ and YZ planes in Case b. The vertical velocity decreases near the edges of the mold cavity. The decrease spreads more in Case a, which is consistent with the larger fill coefficient obtained (1.58 versus 1.31 in Case b).

FIGURE 8 (a) Results of numerical simulations for the existing tool to investigate the relationship between the fill coefficients and preform thickness. As expected, larger preform thicknesses give smaller fill coefficients. (b) Transverse velocity in the cross-section shown by arrows in (a). In each case considered, the velocity is divided equally into 15 color levels from the minimum to the maximum values. As thickness increases, the zones of larger transverse flow velocity become relatively smaller with respect to the whole flow domain.

FIGURE 9 Fill coefficient as a function of an isotropic FDL permeability. The principal permeability of the 4-millimeter-thick isotropic preform is 3.0 x 10-12 m^2.

FIGURE 10 Transverse velocity distribution inside the mold cavity: (a) 3D view obtained by volume rendering for $\boldsymbol{F = 5.1}$. (b) 3D view obtained by volume rendering for $\boldsymbol{F = 1.1}$. (c) Transverse velocity component $\boldsymbol{w}$ along the z-axis for $\boldsymbol{F = 5.1}$. (d) Transverse velocity component $\boldsymbol{w}$ along the z-axis and cross-sectional view of the flow pattern for $\boldsymbol{F = 1.1}$.

FIGURE 11 Typical transverse permeability experimental results obtained with a 1D test device compared with measurements with Flow Distribution Layers (FDL) after correcting for perforated plate deformation.

FIGURE 12 Kriging profiles for parametric surface kriging of the deflection field under a 100 kPa load.

Table list

(a) (b)

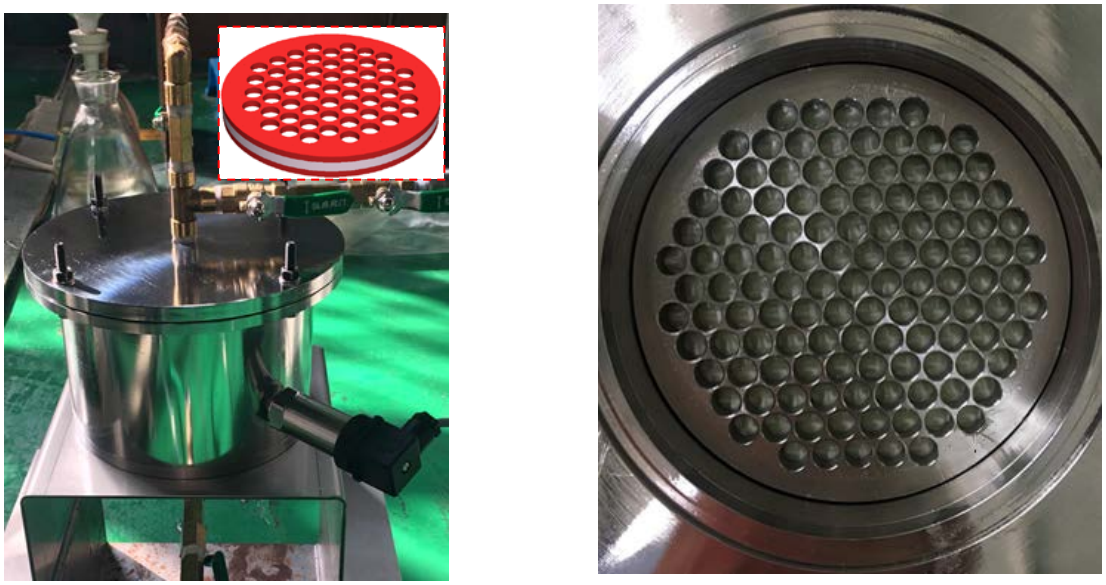

FIGURE 1 Example of one-dimensional transverse permeability test mold: (a) Tool with pressure sensors near the inlet and outlet. (b) Perforated plate.

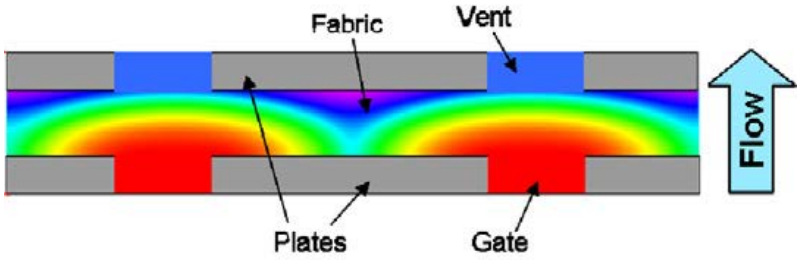

FIGURE 2 The fibrous preform being held between two perforated plates, this figure shows typical non-unidirectional flow patterns created by perforations [10]. Convergent and divergent flows can be observed in zones of the specimen facing impermeable parts in the perforated plates.

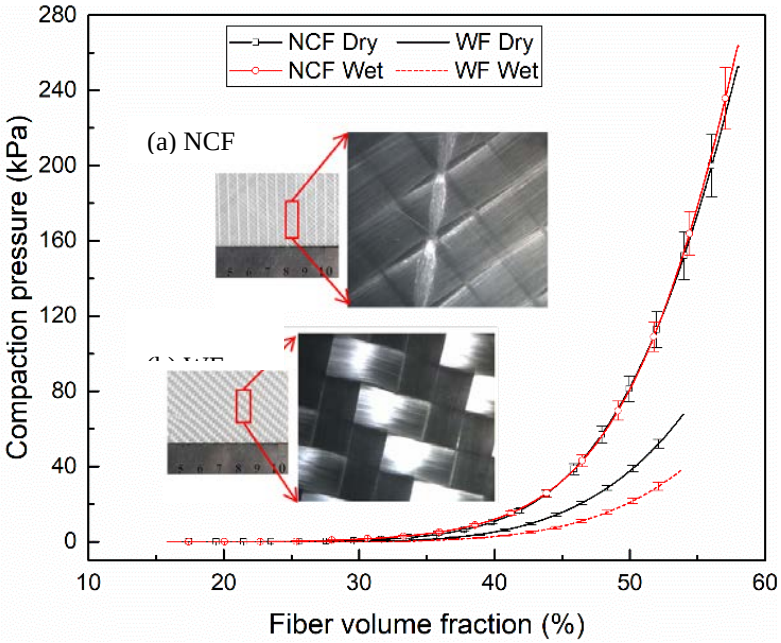

FIGURE 3 Dry and wet compressibility measurement for the two benchmark fabrics (measured at Wuhan University of Technology).

(a)

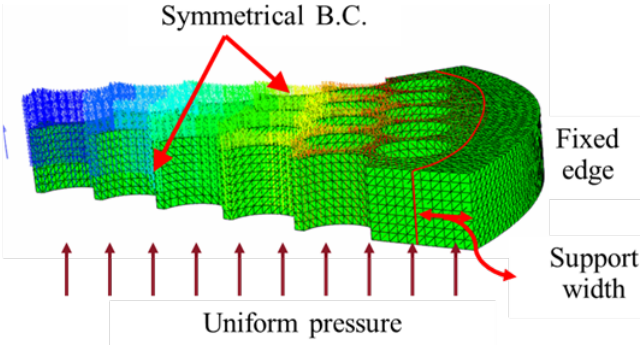

(b)

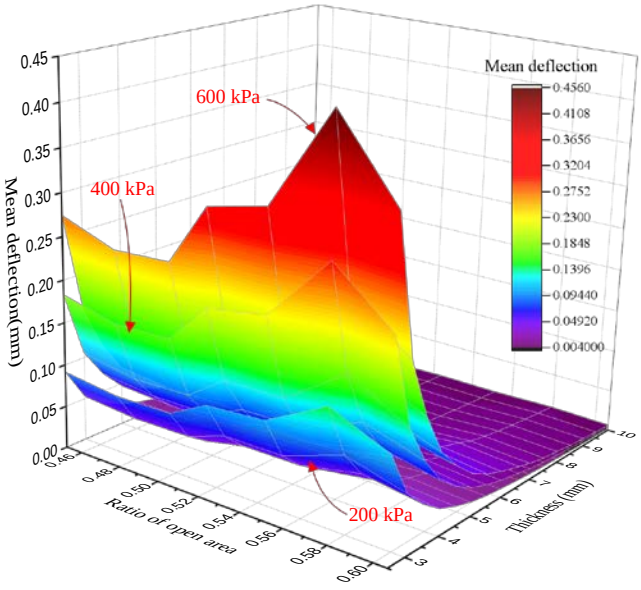

FIGURE 4 Analysis of perforated plate deformation: (a) Boundary conditions for the 3D stiffness finite element analysis of a circular sector. (b) Mean deflection as a function of the open space ratio and plate thickness for the three pressure levels considered (aluminum).

(a) (b)

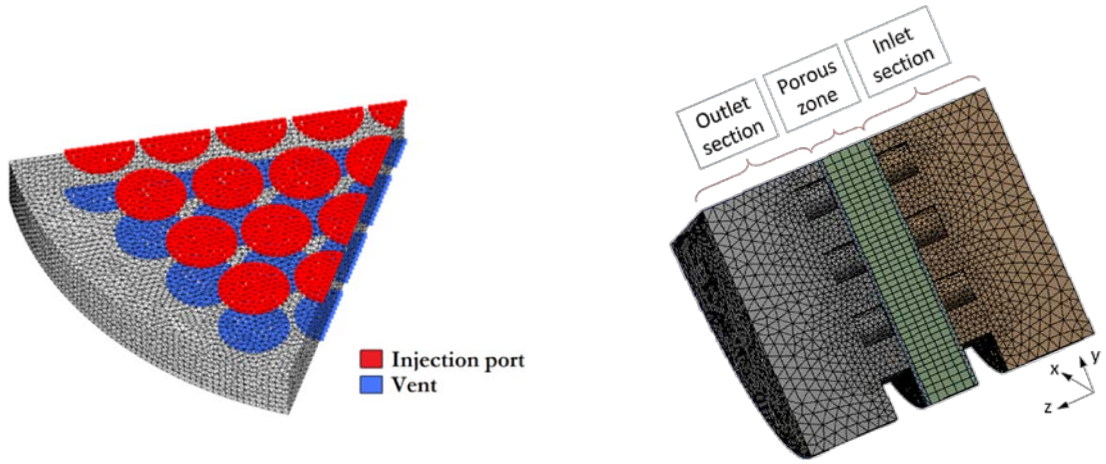

FIGURE 5 Geometrical models and boundary conditions used to conduct filling and saturated flow simulations: (a) Boundary conditions (pressure inlet of 100 kPa in red and outlet at 0 Pa in blue) for filling flow simulations with PAM-RTM. (b) Mesh of the geometrical domain considered for the saturated steady state flow simulations including the preform, the two perforated plates, the FDLs under and above the specimen and part of the inlet and outlet mold cavity. The pressure is 100 kPa in the bottom inlet surface and 0 Pa in the upper outlet surface.

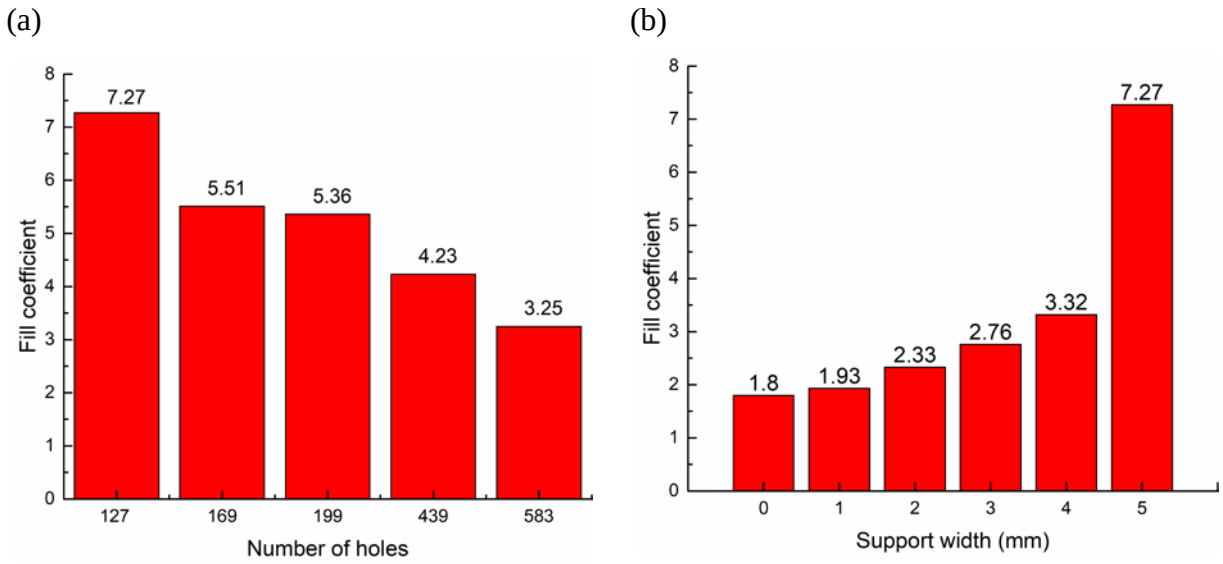

FIGURE 6 Effect of two geometrical parameters on flow patterns for a 7 mm thick preform: (a) Number of perforations for nearly the same open space ratio and reduced hole diameters. (b) Support width (for simulations based on the configuration of Table 1). The decrease in support width is achieved by increasing the inter-hole distance).

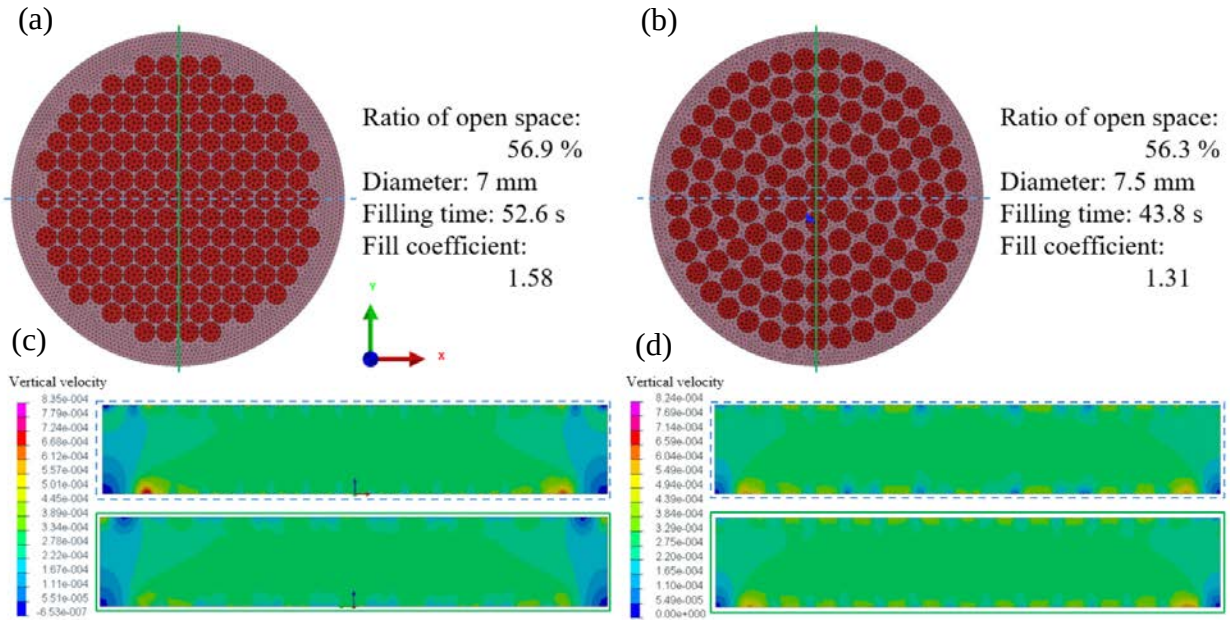

FIGURE 7 Influence of hole packing calculated for a 20 mm thick preform: (a) Non-uniform distribution of perforations near the edge of the mold cavity. (b) Uniformly distributed perforations. (c) Vertical transverse velocity fields in the XZ and YZ planes in Case a. (d) Vertical transverse velocity fields in the XZ and YZ planes in Case b. The vertical velocity decreases near the edges of the mold cavity. The decrease spreads more in Case a, which is consistent with the larger fill coefficient obtained (1.58 versus 1.31 in Case b).

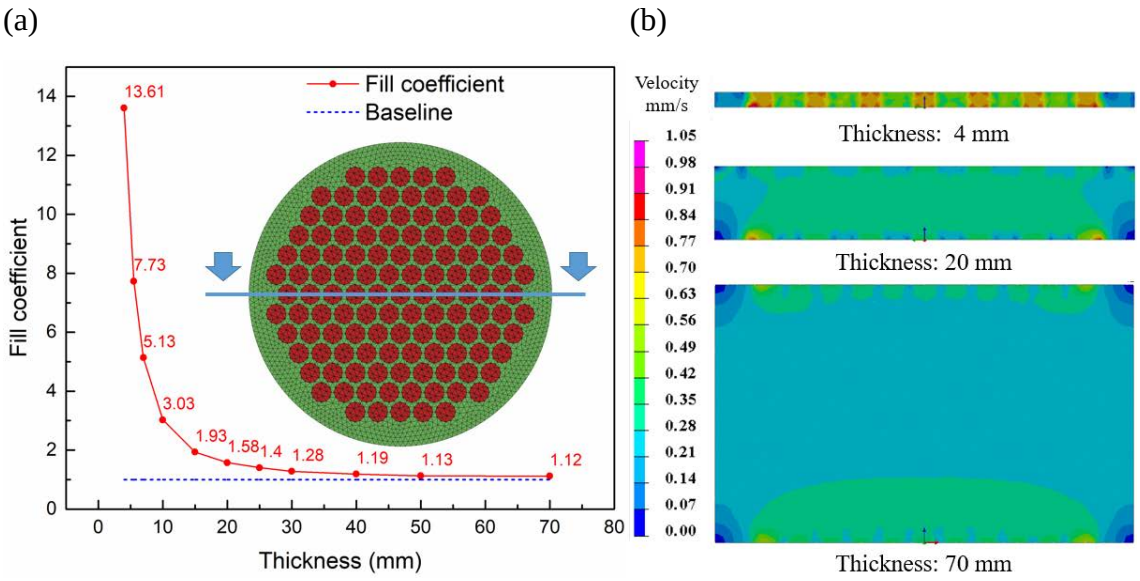

FIGURE 8 (a) Results of numerical simulations for the existing tool to investigate the relationship between the fill coefficients and preform thickness. As expected, larger preform thicknesses give smaller fill coefficients. (b) Velocity magnitude in the cross-section shown by arrows in (a). In each case considered, the velocity is divided equally into 15 color levels from the minimum to the maximum values. As thickness increases, the zones of larger transverse flow velocity become relatively smaller with respect to the whole flow domain and the velocity filed becomes more uniform.

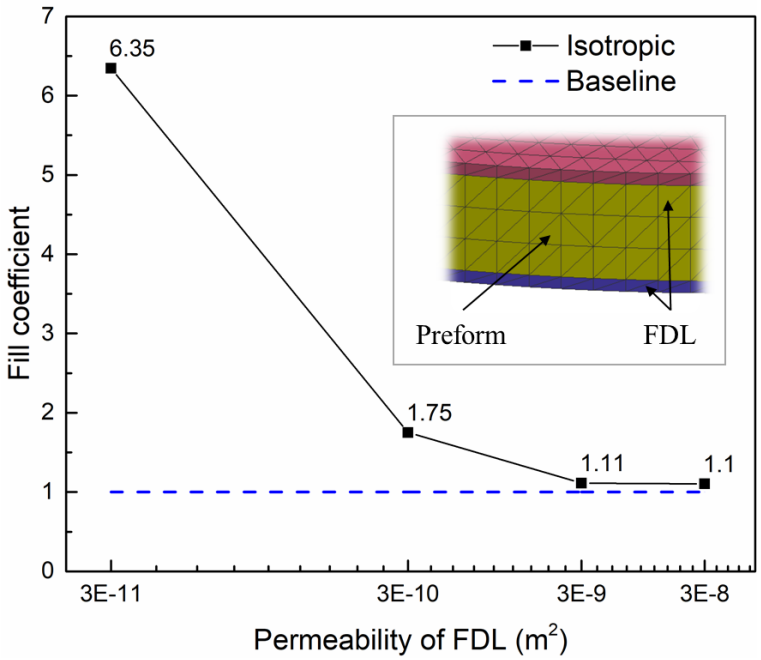

FIGURE 9 Fill coefficient as a function of an isotropic FDL permeability. The principal permeability of the 4-millimeter-thick isotropic preform is 3.0 x 10-12 m^2.

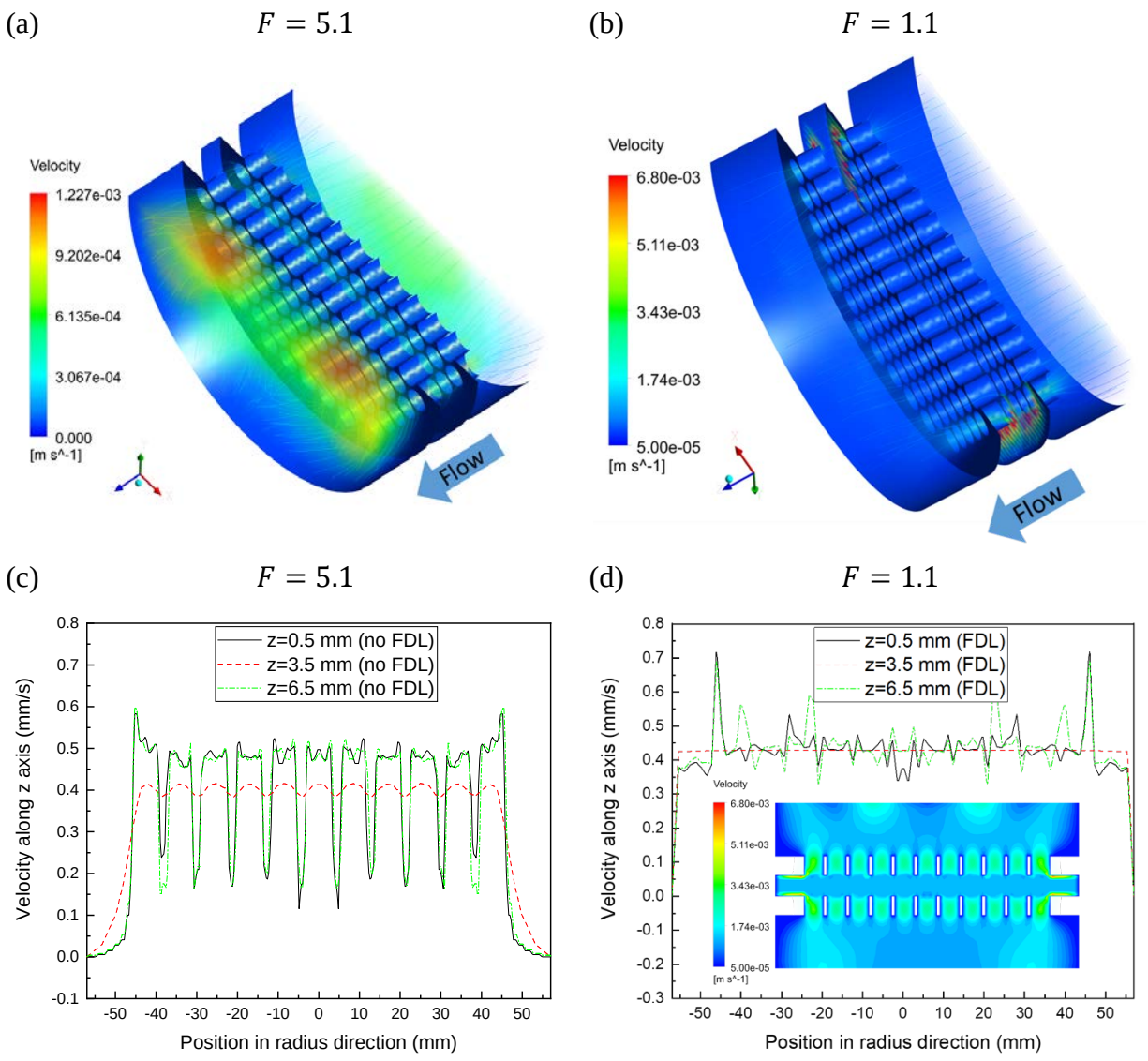

FIGURE 10 Transverse velocity distribution inside the mold cavity: (a) 3D view obtained by volume rendering for $\boldsymbol{F = 5.1}$. (b) 3D view obtained by volume rendering for $\boldsymbol{F = 1.1}$. (c) Transverse velocity component $\boldsymbol{w}$ along the z-axis for $\boldsymbol{F = 5.1}$. (d) Transverse velocity component $\boldsymbol{w}$ along the z-axis and cross-sectional view of the flow pattern for $\boldsymbol{F = 1.1}$.

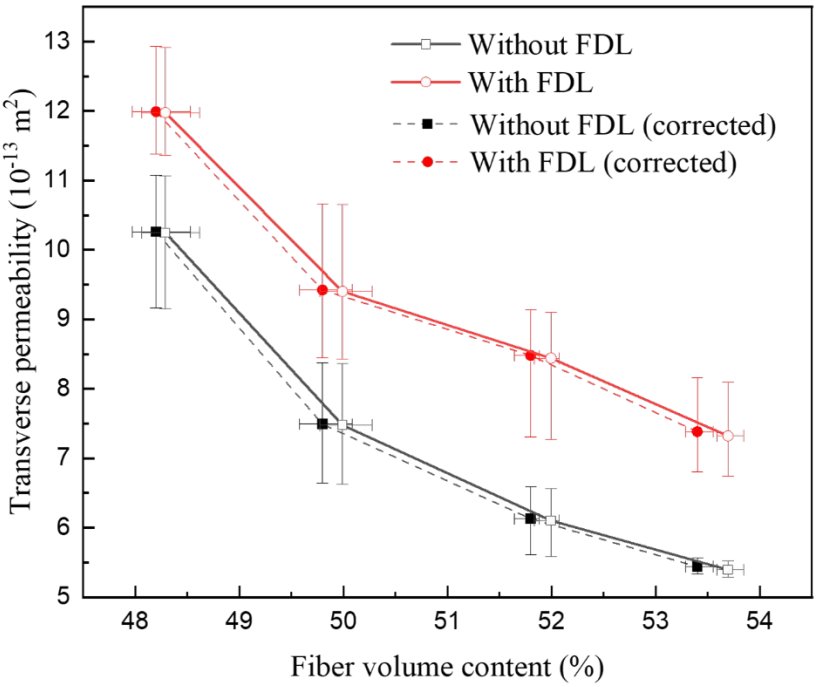

FIGURE 11 Typical transverse permeability experimental results obtained with a 1D test device compared with measurements with Flow Distribution Layers (FDL) after correcting for perforated plate deformation.

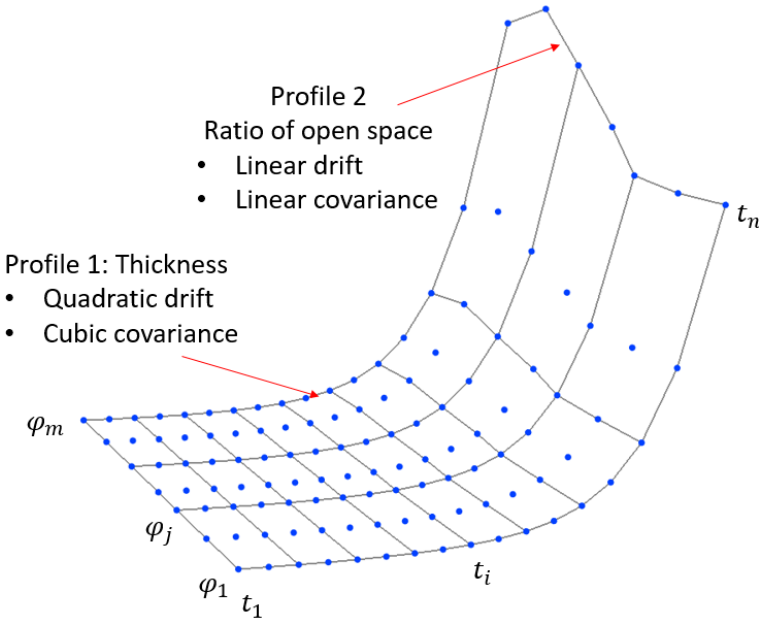

FIGURE 12 Kriging profiles for parametric surface kriging of the deflection field under a 100 kPa load.

Table 1. Configurations of perforated plates reported in the scientific literature

Authors	Material	Shape	Thickness (mm)	Dimension of perforations (mm)	Number of perforations
Visconti et al. [14]	metal net	not specified	0.7	10 * 10 (square)	5
Li et al. [25]	stainless steel	rectangular	10	Φ 5	225
Li et al. [19]	stainless steel	rectangular	not specified	Φ 6 /Φ 2	49/35
Klunker et al. [15]	steel	circular	not specified	Φ 8	95
Huang et al. [13]	stainless steel	circular	6.5	Φ 7.5	60

Table 2. Deflections for similar open space ratios and different perforation patterns

Open space ratio	Hole spacing	Hole diameter	Max. deflection*		Mean deflection*	
			Aluminum	Stainless steel	Aluminum	Stainless steel
55.0 %	8.0 mm	7.5 mm	0.373 mm	0.134 mm	0.074 mm	0.026 mm
54.9 %	7.0 mm	6.5 mm	0.374 mm	0.139 mm	0.076 mm	0.028 mm
55.1 %	6.5 mm	6.0 mm	0.390 mm	0.145 mm	0.085 mm	0.031 mm

Note: * Deflection under 600 kPa acting on the 4-millimeter-thick perforated plate

Table 3. List of simulation cases considered to study the effect of perforations

No.	Hole spacing	Hole diameter	No. of holes	Support width	Open space ratio
1	8.0 mm	7.5 mm	127	5 mm	54.97%
2	7.0 mm	6.5 mm	169	5 mm	54.94%
3	6.5 mm	6.0 mm	199	5 mm	55.12%
4	4.5 mm	4.0 mm	439	5 mm	54.05%
5	4.0 mm	3.5 mm	583	5 mm	54.95%

Table 4. Influence of permeability on the fill coefficient

$K_x = K_y$	K_z	Anisotropy	1D fill time	Actual fill time	Fill coefficient
$3.0\times10^{-11}m^2$	$3.0\times10^{-11}m^2$	1	0.41 s	2.01 s	5.12
$3.0\times10^{-12}m^2$	$3.0\times10^{-12}m^2$	1	4.08 s	20.8 s	5.10
$3.0\times10^{-13}m^2$	$3.0\times10^{-13}m^2$	1	40.8 s	208 s	5.09
$3.0\times10^{-12}m^2$	$3.0\times10^{-13}m^2$	10		63 s	1.54
$3.0\times10^{-11}m^2$	$3.0\times10^{-13}m^2$	100		47.4 s	1.16
$3.0\times10^{-10}m^2$	$3.0\times10^{-13}m^2$	1000		44.0 s	1.08